Volume 1 | Number 1 | Jan 2013 | Pages 1–100

Journal of
Materials Chemistry A

Materials for energy and sustainability
www.rsc.org/materialsA

Li⁺

ROYAL SOCIETY
OF CHEMISTRY

ROYAL SOCIETY
OF CHEMISTRY

www.rsc.org/materialsA

Workfunction, a new viewpoint to understand the electrolyte/electrode interface reaction

Yurui Gao, Zhaoxiang Wang*, and Liquan Chen

Abstract

Severe gassing during cycling hinders the application of spinel $Li_4Ti_5O_{12}$, a zero-strain anode material for constructing high power-density and long-lifespan Li-ion batteries. The gassing issue is caused by the interface reaction between $Li_4Ti_5O_{12}$ and the electrolyte. This article tries to understand the $Li_4Ti_5O_{12}$/electrolyte interface reaction and the chemical stability of $Li_4Ti_5O_{12}$ from a new viewpoint, the surface workfunction, the energy required to take away one electron from the Fermi level. Density functional theory (DFT) calculations indicate that the workfunction decreases due to the presence of Li-rich surface (Li^+-occupied 16c sites) of $Li_{3+x}Ti_{6-x}O_{12}$. Meanwhile, the chemical potential rises and even reaches the LUMO of the carbonate electrolyte, easily inducing interface reactions. This means that the electrochemically lithiated phase $Li_7Ti_5O_{12}$ is responsible for the electrolyte decomposition on the surface. The Li-rich surfaces of $Li_4Ti_5O_{12}$ generated during material preparation or chemical lithiation can also trigger the interface reactions. In combination of the experimental and calculational results, we believe that the interface reaction involves losses of electrons and Li^+ ions from the Li-rich surface of $Li_4Ti_5O_{12}$ or $Li_7Ti_5O_{12}$, and the reduction of the electrolyte. In addition, O vacancies on the surface decrease the workfunction and further promote the reaction.

1. Introduction

As Li-ion batteries (LIBs) have been widely applied in electric vehicles, developing electrode materials with high energy-density, high power-density and long lifespan is urgently required.[1] Spinel $Li_4Ti_5O_{12}$ ($Fd\overline{3}m$) is the end member of the spinel titanate family, $Li_{3+x}Ti_{6-x}O_{12}$ (0≤x≤1). These materials firstly drew attention for their superconductivity at a relatively high transition temperature and then for their capability of storing Li ions as an anode material for Li-ion batteries.[2,3] In $Li_4Ti_5O_{12}$ (Fig. 1), 3/4 of the Li^+ ions occupy the 8a sites while the other Li^+ ions and all the Ti ions stay on the 16d sites at a ratio of 1:5, and the O^{2-} ions occupy the 32e sites. Therefore, $Li_4Ti_5O_{12}$ can be more precisely written as $[Li_3]_{8a}\square_{16c}[LiTi_5]_{16d}[O_{12}]_{32e}$, with the 16c sites unoccupied.[4-6] Similar to the case of the pure spinel $LiTi_2O_4$ (x=0),[7] Li^+ ions are inserted into the empty 16c sites accompanied with Li^+ ion migration from the 8a to the 16c sites.[8-11] This migration leaves the 8a sites empty and leads to phase transition from $[Li_3]_{8a}\square_{16c}[LiTi_5]_{16d}[O_{12}]_{32e}$ to $\square_{8a}[Li_6]_{16c}[LiTi_5]_{16d}[O_{12}]_{32e}$ but with negligible volume change.[4-6] With its "zero-strain" property, high rate capability and excellent cycling stability, $Li_4Ti_5O_{12}$ is an alternative to the graphitic anode materials for high power LIBs.[12-14]
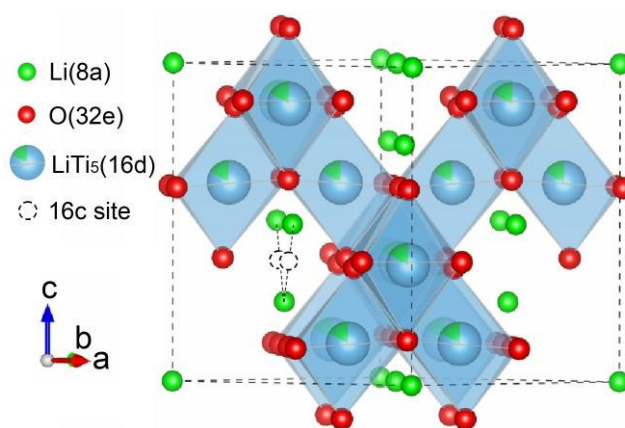
Fig. 1 The schematic structure of spinel $Li_4Ti_5O_{12}$ ($Fd\overline{3}m$, z=227, a=b=c= 8.3588 Å).

However, after decades of studies, the $Li_4Ti_5O_{12}$ anode still has not been successfully applied in large scale, mainly due to the aggressive gassing and severe battery swelling during charge/discharge processes. There have been experimental studies on its gassing issue.[15-17] The gases inside the $Li_4Ti_5O_{12}$ cell are dominantly H_2 as well as CO_2, CO, CH_4, and C_2H_4.[15,16] In addition, the inflation rate is correlated with the storage temperature by an Arrhenius-type curve.[16] In order to suppress or eliminate the gassing, it is critical to understand the gassing mechanism in $Li_4Ti_5O_{12}$. As very little gas has been detected inside the carbon-based cells, the large amount of gas generated in $Li_4Ti_5O_{12}$ cell cannot just be attributed to the presence of trace amount of moisture in the electrolyte or the active materials. In addition, the gassing was found in $Li_4Ti_5O_{12}$-based cells stored at room temperature.[17] Therefore, interface reactions related to the surface structure of $Li_4Ti_5O_{12}$ and/or its derivatives are supposed to be responsible for the gassing issue. Yang *et al.*[17] pointed out that $Li_4Ti_5O_{12}$ instead of PF_5 is the initiator of such interface reactions. That is, the change of surface plane from (111) to (222) and the formation of TiO_2 (101) plane are responsible for these reactions. These findings are helpful for understanding the gassing issue, but cannot answer why $Li_4Ti_5O_{12}$ reacts with the electrolyte. The detailed/fundamental reaction mechanism (reduction or oxidation) remains unclear.

The workfunction (Φ), critical for understanding the field-emission property of a metal, is usually defined as the energy required to take away one electron from the Fermi level μ , $\Phi = \phi - \mu$, where ϕ refers to the vacuum level.[18,19] Therefore, it is potentially able to express the capability of electron loss from the surface of

$Li_4Ti_5O_{12}$. With the concept of surface workfunction, the chemical stability of $Li_4Ti_5O_{12}$ immersed in the electrolyte can be evaluated and the process of the detailed redox reaction between $Li_4Ti_5O_{12}$ and the electrolyte can be predicted or understood.

The interface reaction is closely related with the surface structure of $Li_4Ti_5O_{12}$. We previously investigated the stability of $Li_4Ti_5O_{12}$ in air by a series of physical and electrochemical techniques and observed Li_2CO_3 on the surface of $Li_4Ti_5O_{12}$.[20] Density functional theory (DFT) calculations on the surface structure of $Li_4Ti_5O_{12}$ showed that its surface is Li-rich and prefers to be Li-truncated, explaining why the surface tends to absorb H_2O and CO_2 to form Li_2CO_3. In this work, we study the gassing-related issues, the interface reaction between $Li_4Ti_5O_{12}$ and the carbonate-based electrolyte solution system, based on the DFT calculated surface workfunction. It is suggested that the oxygen vacancies on the surface cannot trigger the reaction but the Li-rich property of the spinel $Li_{3+x}Ti_{6-x}O_{12}$ surface can easily introduce interface reactions, transferring electrons from the Li-rich surface of $Li_4Ti_5O_{12}$ or $Li_7Ti_5O_{12}$ to the electrolyte system. These interface reactions are confirmed with Fourier-transformed infrared (FTIR) spectroscopic analysis and quasi "potentiostatic" discharge test.

2. Method

The spin-polarized calculations[21,22] were performed based on DFT, implemented with the Vienna *ab initio* simulation package (VASP).[23] Pseudopotentials were established by the projector-augmented wave (PAW)[24] method with generalized gradient approximation (GGA) by Perdew-Burke-Ernzerh (PBE)[25] as the exchange-correlation

functional. The Li (2s, 2p), O (2s, 2p) and Ti (3d, 4s) orbitals were treated as the valence states. The plane-wave cutoff energy was 500 eV. The investigations by Wang et al.[26], Lutfalla et al.[27] and Hu et al.[28] showed that although the Ti-3d electrons were thought to be weakly localized, the DFT error cannot be ignored in redox calculation according to the redox energy comparison. Therefore, in order to compensate for the DFT error in the calculation of the Ti-3d electrons, the Hubbard-type U[29] calibration is still required. According to the reports of Lutfalla et al.[27] and Hu et al.[28], U_{eff} was set to be 2.5 eV (U=3.5 eV, J=1.0 eV). Symmetrical surfaces were established with 7 layers of TiO_6 octahedron, sufficient to make the surface energy convergent. The thickness of the slab was 42.18 Å with a 25 Å vacuum layer.[20] A $3 \times 3 \times 1$ Monkhorst-Pack k-point mesh was adopted to relax all the atoms until the Hellmann-Feynman force became less than 0.01 eV $Å^{-1}$. As for the static calculations, a denser k-point mesh of $5 \times 5 \times 1$ was employed.

3. Results and discussion

3.1 O vacancy on the surface

As the $Li_4Ti_5O_{12}$ (111) plane is always exposed to air or vacuum[20] and the interface reaction is believed to be related with the (111) surface,[17] we take this plane as the object of this work. As the $Li_4Ti_5O_{12}$ (111) surface is complex and $Li_4Ti_5O_{12}$ is the end member of the spinel family $Li_{3+x}Ti_{6-x}O_{12}$ (0≤x≤1), in order to simplify the calculation model, we adopt the (111) plane of spinel $LiTi_2O_4$ (x=0 in $Li_{3+x}Ti_{6-x}O_{12}$) as the initial model to have an extensive study on this lithium titanate family. The obtained results will also be true for $Li_4Ti_5O_{12}$ (x=1) because the surfaces of both $Li_4Ti_5O_{12}$ and

LiTi$_2$O$_4$ are Li-truncated.[20]

The entire local potential is composed of the electrostatic and the exchange correlation parts. The exchange correlation potential always presents strong oscillations and thus leads to fluctuation of the entire local potential in the vacuum (Fig. S1). Therefore, only the electrostatic part is used to evaluate the workfunction. Fig. 2a shows the corresponding workfunction of LiTi$_2$O$_4$ obtained by calculating the difference of one electron on the vacuum level (in the vacuum slab) from that on the Fermi level. The thickness of the vacuum slab is 25 Å, sufficient to make the workfunction convergent with a fluctuation of less than 0.01 eV (Fig. S2). The vacuum level is located in the deep vacuum slab and is calculated as the average electrostatic potential energy on the plane of z along the c direction. It becomes convergent at z=30.759 Å. The energy fluctuation (Fig. 2b) is within 0.01 eV. Therefore, the obtained vacuum level ϕ is acceptable.
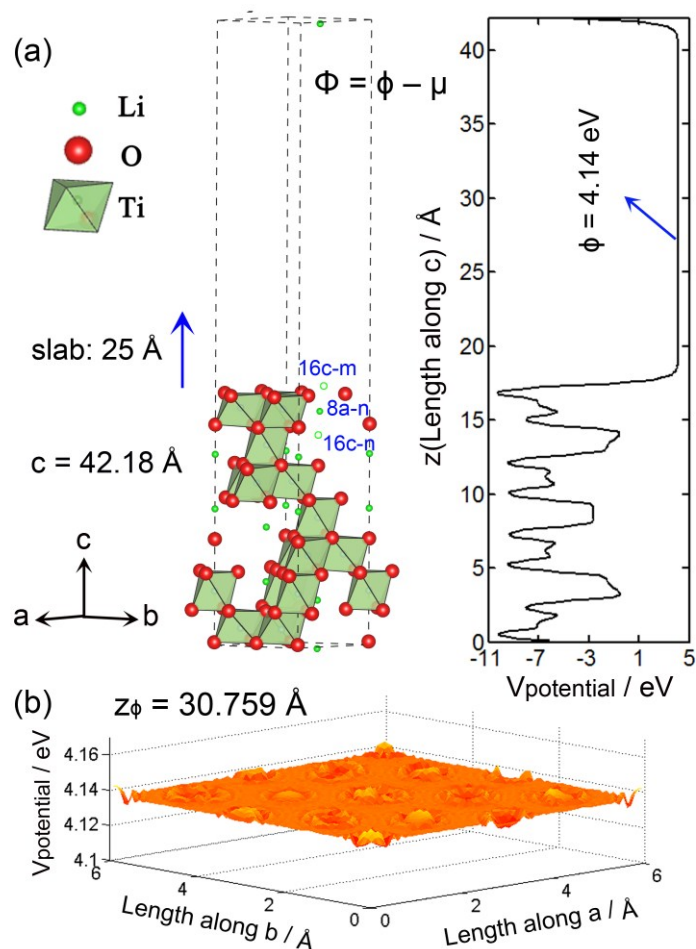
Fig. 2 (a) Planar average of the electrostatic potential energy along the *c* direction of the LiTi$_2$O$_4$ (111) surface (for ease of description, the 16c sites at the outmost surface and next to the outmost surface are denoted as 16c-m and 16c-n, respectively, and the 8a site next to the outmost surface as 8a-n. Herein, the Li ions occupy the 8a sites while the 16c-m and 16c-n sites are empty in the model); (b) the energy fluctuation of the vacuum level on the selected plane (z = 30.759 Å along *c*) in the vacuum slab.

Table 1. Workfunction and atomic population of Ti on the LiTi$_2$O$_4$ (111) surface (Fig. 2a) with *y* as the coverage of O vacancy.

Y	0	0.25	0.5	0.75
ϕ / eV	4.14	3.78	3.56	3.16
μ / eV	-2.25	-1.48	-1.42	-1.01
Φ / eV	6.39	5.26	4.98	4.17

Population: Ti1	1.371	1.584	1.908	1.992
Ti2	1.371	1.368	1.576	1.998
Ti3	1.371	1.584	1.908	2.124

Note: Ti1, Ti2 and Ti3 are three Ti ions on the surface.
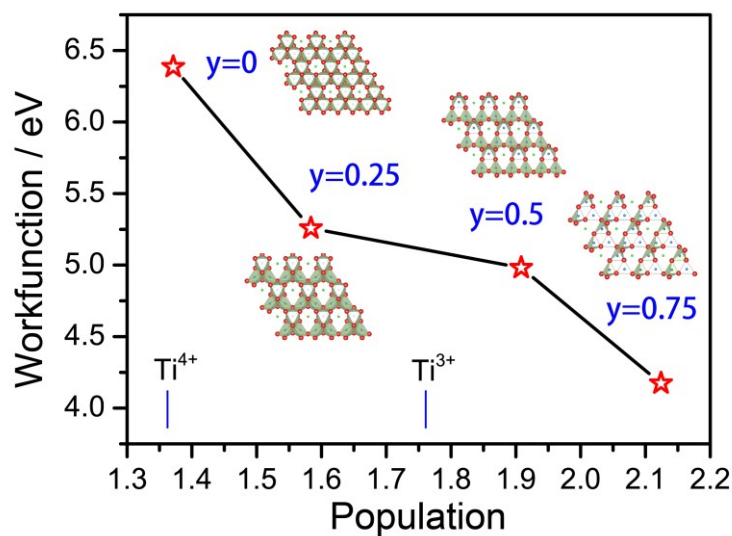
Fig. 3 Workfunction modulated with the coverage (*y*) of O vacancies on the surface. The *x* axis reflects the highest atomic population of Ti on the surface.

Table 1 shows the workfunction and atomic population, obtained by Bader analysis, of Ti on the surface. The valence state of Ti on the surface can be determined according to its population. As our calculation results show that the population of Ti is 1.76 in $LiTiO_2$ and 1.33 in TiO_2 (See the Supporting Information for details), the population for the Ti^{3+} and Ti^{4+} is treated as 1.76 and 1.33, respectively. The original $LiTi_2O_4$ (111) plane truncated surface (without extra Li^+ ions shown in Fig. 2a) tends to contain Ti^{4+}. The states near the Fermi level is mainly the contribution of the Ti ions in the bulk, shown from the real-space distribution of the charge close to the Fermi level (Fig. S3). In this case, the workfunction is 6.39 eV. However, the

workfunction decreases when O vacancies come into being. When the coverage of the

O vacancies on the surface reaches 0.25, the valence state of the Ti ions decreases to

somewhere between Ti^{3+} and Ti^{4+}, and the workfunction becomes 5.26 eV. The states

near the Fermi level is derived from the Ti atoms on the surface as well as those in the

bulk (Fig. S3). As more O vacancies appear, the Ti-3d electrons on the surface

contribute more states near the Fermi level. In addition, the valence of the Ti on the

surface becomes lower and the workfunction becomes smaller. Therefore, the

workfunction of the spinel lithium titanate is modulated by the coverage of the O

vacancies on the surface (Fig. 3). That is, the presence of the O vacancies on the

surface increases the electrons on the surface Ti ions, resulting in the presence of Ti^{3+}

or Ti ions with even lower valences. As a result, the workfunction decreases, easing

the loss of electrons on the surface.

By comparing the chemical potential with the electrochemical window of the

electrolyte, the chemical stability of $Li_{3+x}Ti_{6-x}O_{12}$ towards the electrolyte and the

possible redox reaction between $Li_{3+x}Ti_{6-x}O_{12}$ and the electrolyte can be

characterized.[30] Herein, the chemical potential can be simply understood as the Fermi

level of electrons in the surface system referring to the vacuum level. The

electrochemical window of the electrolyte is determined by the highest occupied

molecular orbital (HOMO) and the lowest unoccupied molecular orbital (LUMO) of

all the molecules in the electrolyte system. Considering that the commonly used

electrolyte ($LiPF_6$ dissolved in a mixture of ethylene carbonate and dimethyl

carbonate) is reduced below 0.8 V and oxidized above 5.0 V *vs*. Li^+/Li, the HOMO

and LUMO values of the electrolyte are all calculated referring to that of Li metal in this work. Since the Li metal surface shows random crystallographic orientation and the orientation is largely affected by the rolling of the Li sheet, we adopted the average workfunction of the 5 low-index surfaces {100}, {110}, {111}, {210} and {211} to access the positions of the LUMO and HOMO of the electrolyte. The average workfunction of Li metal is calculated to be 2.76 eV (See the Supporting Information). If the vacuum level is defined as 0 eV, then the chemical potential of Li (111) will be -2.76 eV. Therefore, the LUMO and HOMO values of the commonly used electrolyte are ca. -3.56 and -7.76 eV, respectively. Correspondingly, the surface chemical potentials of $LiTi_2O_4$ (111) with different coverages (y = 0, 0.25, 0.5 and 0.75) of O vacancies are -6.39, -5.26, -4.98 and -4.17 eV, respectively. Fig. 4a shows that the chemical potentials of the electrons from O-vacancy containing surfaces are all well within the electrochemical window of the electrolyte. Therefore, the interface chemical interaction will not occur. However, the O vacancies on the surface make the chemical potential increase towards the LUMO of the electrolyte.
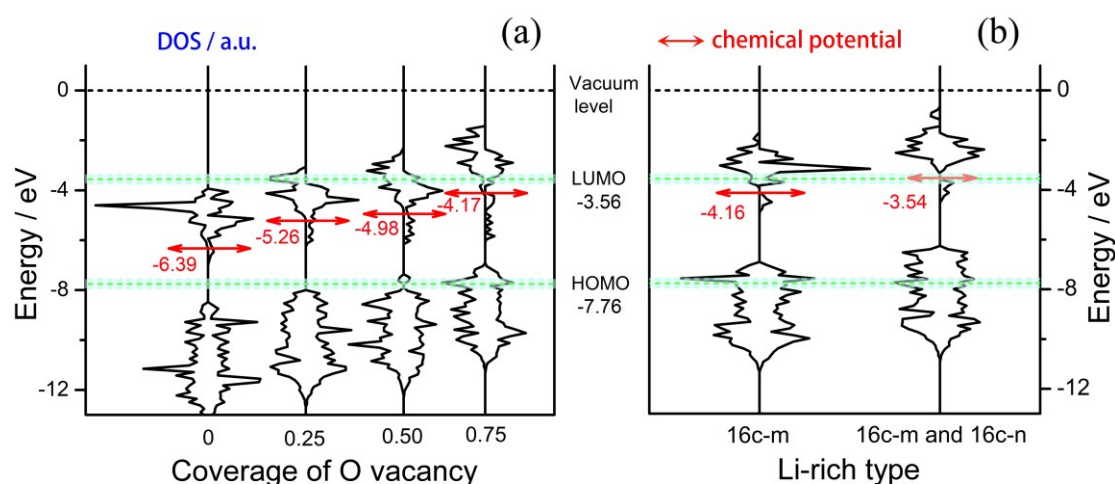
Fig. 4 Density of states (DOS) for the $LiTi_2O_4$ (111) surface (a) with different coverages of O

vacancies displaying the chemical potentials well within the electrochemical window of the electrolyte, and (b) with different Li-rich states indicating the chemical potential close to and even reaching the LUMO of the electrolyte. The light green areas are for the fluctuation ranges of the LUMO and HOMO of the electrolyte due to the variation of referred Li surfaces. The band gap is 0.24 eV for the surface with the Li$^+$ ions occupying the 16-m and 16c-n sites. All energies refer to the vacuum level.

3.2 Li-rich surface

The surface of Li$_{3+x}$Ti$_{6-x}$O$_{12}$ is Li-rich.[20] Since the formation energy (see the Supporting Information for the detailed definition) of one lithium atom occupying the 16c-m site is -2.92 eV, the 16c site at the outmost surface tends to be occupied with Li$^+$ ions. In this case, the Li$^+$ ions on the 8a-n sites are relaxed to the 16c sites most likely due to the Coulombic repulsion between the Li$^+$ ions on 16c-m site, and the Li$^+$ ions on 8a-n site only ~1.83 Å away from the former. Meanwhile, the workfunction decreases from 6.39 eV to 4.16 eV. The atomic Bader analysis (Table S1) shows that the Ti^{4+} ions are on the surface while the Ti^{3+} ions are located only in the bulk. The electrons near the Fermi level are mainly the contribution of the Ti-3d orbit in the bulk (Fig. S4a).

With the 16c-m sites occupied with the Li$^+$ ions, the 16c-n sites tend to be further occupied with the Li$^+$ ions for a lithium-richer surface with formation energy (see the Supporting Information for the detailed definition) of -0.97 eV, close to the energy of lithium insertion into the bulk LiTi$_2$O$_4$. Such Li-rich surface is possible if excess Li is added upon material synthesis. In this case, the Ti^{3+} ions appear on the surface, the workfunction decreases to 3.54 eV and the electrons near the Fermi level are mainly the contribution of Ti-3d orbit on the surface as well as small portion in the bulk (Fig. S4b).

Fig. 4b compares the density of states (DOS) with the electrochemical window of the carbonate-based electrolyte. After attributing the vacuum level to zero, the Fermi level of the above two kinds of Li-rich surfaces are located at -4.16 and -3.54 eV, respectively. The latter is even 0.02 eV higher than the LUMO of the electrolyte. Moreover, considering the energy excitation by temperature (ca. 0.026 eV at 300 K), it is easy for the electrons near the Fermi level on the second kind of Li-rich surface (with 16c-m and 16c-n sites occupied by Li^+ ions) to jump onto the LUMO of the electrolyte and thus trigger the interface reaction between the Li-rich surface and the electrolyte. According to this, the lithiated phase $Li_7Ti_5O_{12}$ is mostly responsible for the electrolyte decomposition on the surface and the resultant gassing in the cell, well consistent with the previous reports that the $Li_4Ti_5O_{12}$ full cells swell after storage at a full-charge state.[15-17] On the other hand, the Li-rich surfaces of $Li_4Ti_5O_{12}$ generated during material preparation or chemical lithiation can also trigger interface reactions. In addition, the rate of the interface reaction is determined with the electron transition probability that has an Arrhenius-type dependence on the temperature, leading to the Arrhenius-type correlation between the swelling of the cell and the storage temperature, in good agreement with previous report.[16]

Some difference might arise in the calculation results when spinel $LiTi_2O_4$ is taken for $Li_4Ti_5O_{12}$. From the structural point of view, the difference between $LiTi_2O_4$ and $Li_4Ti_5O_{12}$ lies in species occupying the 16d sites. In $LiTi_2O_4$, the 16d sites are all occupied with Ti ions while only 5/6 of the 16d sites are occupied with Ti ions (the other 1/6 sites are occupied by Li^+ ions) in $Li_4Ti_5O_{12}$. Such occupation will not affect

the occupancy of the Li^+ ions or the charge distribution at the surface if it occurs in

the bulk far from the surface. If it takes place in the TiO_6 octahedral block close to the

surface, the Li^+ ions at the outmost surface will not be affected either, due to the

shielding effect of the TiO_6 block at the outmost surface. Although the charge

distribution on the surface might be affected, insertion of more Li^+ ions into the 16c

and the migration of Li^+ ions from the 8a to 16c sites, corresponding to the case of

$Li_7Ti_5O_{12}$, can compensate for the difference of Ti/Li occupancy on the 16d sites and

its impact on the charge of surface Ti. If the Li^+ ions occupy the 16d sites in the

outmost TiO_6 block, the formation energy will be higher than that of the occupation

on the internal 16d sites. Therefore, the above results are applicable to $Li_4Ti_5O_{12}$ as

well.

3.3 Experimental section

Fig. 5 compares the FTIR spectra of the fresh and cycled $Li_4Ti_5O_{12}$ electrodes (63

cycles) between 1.0 and 2.5V. Vibration peaks of Li_2CO_3[20] appear at 870, 1433 and

1489 cm^{-1} after cycling. Therefore, one of the products of the interface reaction is

Li_2CO_3.
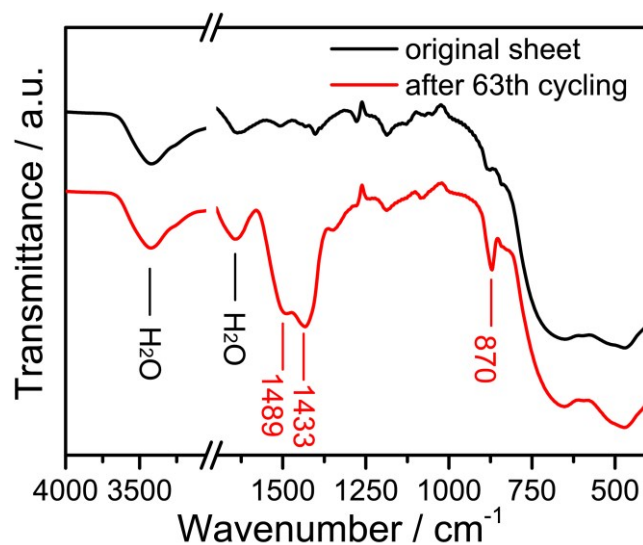
Fig. 5 FTIR spectra of $Li_4Ti_5O_{12}$ sheet before cycling and after 63 cycles. The peaks at 3424 and 1644 cm^{-1} are assigned to the absorbed water during sample preparation (tabletting and transferring).

Quasi "potentiostatic" discharge was conducted to have the $Li_4Ti_5O_{12}$ cell discharged to 1.0 V as much as possible. The cell was firstly discharged to 1.0 V at a rate of 0.02 C and then stood by for 3h. When its voltage rose to above 1.06 V, the galvanostatic discharge was started at the same rate until the cell voltage lowered to 1.0 V. The cell then stood by for another 3h. This process was repeated until the voltage rise was smaller than 0.06 V in 3 h. With this, it is supposed that $Li_4Ti_5O_{12}$ has been completely transformed to $Li_7Ti_5O_{12}$. This cell was later stored in a 50 °C oven. After 15 days, the voltage of the cell was found to have recovered to 1.5V, indicating the coexistence of two phases, $Li_4Ti_5O_{12}$ and $Li_7Ti_5O_{12}$. In addition, Li_2CO_3 was detected by FTIR spectroscopy. This means that Li_2CO_3 can be formed during discharge. Moreover, the specific capacity obtained from the repeated discharge and stand-by of the cell was 231 mAh g^{-1}, higher than the theoretical capacity of $Li_4Ti_5O_{12}$, 175 mAh g^{-1}. The difference between the actual and theoretical capacities is attributed

to the reaction between the Li-rich $Li_7Ti_5O_{12}$ surface and the electrolyte. This simultaneous surface reaction results in the transition from $Li_7Ti_5O_{12}$ to $Li_4Ti_5O_{12}$ in the surface area and the decomposition of the electrolyte. The above recognized Li_2CO_3 is one of the decomposition products of the electrolyte. With the repeated discharge and stand-by processes, the electrolyte decomposition products are accumulated and slow down the surface reaction. However, the surface reaction does not stop even after the cell is removed from the battery tester and transferred into the oven. Therefore, the voltage of the cell restores to 1.5 V after storage of 15 days in the oven. In this process, $Li_7Ti_5O_{12}$ loses electrons to the electrolyte for the surface reaction.

The above analysis demonstrates the necessity to increase the electrochemical window, especially the LUMO, of the electrolyte, determined with the salt, additives and the solvent. On the other hand, as the interface reaction is initiated with the Li-rich surface, surface coating that functions to separate the electrolyte from the active materials should be another effective way to suppress the interface reactions between the $Li_{3+x}Ti_{6-x}O_{12}$ and the electrolyte.

4. Conclusions

In conclusion, DFT calculations are conducted to obtain the surface workfunction of $Li_{3+x}Ti_{6-x}O_{12}$ (111) plane. Based on the calculations, the chemical potential is obtained by referring to the vacuum level and is compared with the electrochemical window of the commonly used commercial electrolytes. It indicates that the O vacancies on the surface decrease the workfunction and promote the interface reaction but cannot

trigger the reaction since the chemical potential of the surface with a large number of O vacancies is well within the electrochemical window of the electrolyte. On the other hand, the Li-rich surface (Li occupying on the 16c sites) of $Li_{3+x}Ti_{6-x}O_{12}$ make the workfunction smaller and the chemical potential close to or even reach the LUMO of the electrolyte, especially when with the assistance of temperature excitation. Therefore, the Li-rich surface of $Li_{3+x}Ti_{6-x}O_{12}$ easily loses electrons to, and reacts with, the electrolyte. According to these calculations, the lithiated phase $Li_7Ti_5O_{12}$ in the surface area seems most responsible for the gassing of the $Li_4Ti_5O_{12}$ cells. Meanwhile, the Li-rich surface of $Li_4Ti_5O_{12}$ introduced during material preparation or chemical lithiation by the environment can also trigger the interface reaction. Combined with the experimental cell tests and FTIR spectroscopic analysis, the interface reaction involves oxidation of the Li-rich surface of $Li_4Ti_5O_{12}$ or $Li_7Ti_5O_{12}$ and the reduction of the electrolyte, with Li_2CO_3 as one of the reaction products. Our work takes a substantial step from a new point of view in understanding and reaching the gassing issue of $Li_4Ti_5O_{12}$ cell. These findings will provide important guidance to the applications of $Li_4Ti_5O_{12}$ and the $Li_{3+x}Ti_{6-x}O_{12}$ spinel family in high power-density Li-ion batteries.

Conflict of interest

The authors declare no competing financial interests.

Acknowledgments

Notes and References

Key Laboratory for Renewable Energy, Beijing Key Laboratory for New Energy Materials and Devices, Beijing National Laboratory for Condensed Matter Physics, Institute of Physics, Chinese Academy of Sciences, P. O. Box 603, Beijing 100190, China. Email: zxwang@iphy.ac.cn Tel: +86-10-82649050 Fax: +86-10-82649050.

† Electronic Supplementary Information (ESI) is available.

References

1　J. -M. Tarascon and M. Armand, *Nature*, 2001, **414**, 359.

2　E. Ferg, *J. Electrochem. Soc.*, 1994, **141**, L147.

3　W. J. H. Borghols, M. Wagemaker, U. Lafont, E. M. Kelder and F. M. Mulder, *J. Am. Chem. Soc.*, 2009, **131**, 17786.

4　T. Ohzuku, A. Ueda and N. Yamamoto, *J. Electrochem. Soc.*, 1995, **142**, 1431.

5　M. Wagemaker, D. R. Simon, E. M. Kelder, J. Schoonman, C. Ringpfeil, U. Haake, D. Lützenkirchen-Hecht, R. Frahm and F. M. Mulder, *Adv. Mater.*, 2006, **18**, 3169.

6　X. Lu, L. Zhao, X. He, R. Xiao, L. Gu, Y. S. Hu, H. Li, Z. Wang, X. Duan, L. Chen, J. Maier and Y. Ikuhara, *Adv. Mater.*, 2012, **24**, 3233.

7　M. Wagemaker, A. Van Der Ven, D. Morgan, G. Ceder, F. M. Mulder and G. J.

Kearley, *Chem. Phys.*, 2005, **317**, 130.

8　G.-N. Zhu, H.-J. Liu, J.-H. Zhuang, C.-X. Wang, Y.-G. Wang and Y.-Y. Xia, *Energy Environ. Sci.*, 2011, **4**, 4016.

9　L. Cheng, J. Yan, G.-N. Zhu, J.-Y. Luo, C.-X. Wang and Y.-Y. Xia, *J. Mater. Chem.*, 2010, **20**, 595.

10　M. Wilkening, W. waniak, J. Heine, V. Epp, A. Kleinert, M. Behrens, G. Nuspl, W. Bensch and P. Heitjans, *Phys. Chem. Chem. Phys.*, 2007, **9**, 6199.

11　M. Wagemaker, E. R. van Eck, A. P. Kentgens and F. M. Mulder, *J. Phys. Chem. B*, 2009, **113**, 224.

12　L. Aldon, P. Kubiak, M. Womes, J. C. Jumas, J. Olivier-Fourcade, J. L. Tirado, J. I. Corredor and C. P. Vicente, *Chem. Mater.*, 2004, **16**, 5721.

13　L. Zhao, Y. S. Hu, H. Li, Z. Wang and L. Chen, *Adv. Mater.*, 2011, **23**, 1385.

14　K.-S. Park, A. Benayad, D.-J. Kang and S.-G. Doo, *J. Am. Chem. Soc.*, 2008, **130**, 14930.

15　I. Belharouak, G. M. Koenig, T. Tan, H. Yumoto, N. Ota and K. Amine, *J. Electrochem. Soc.*, 2012, **159**, A1165.

16　K. Wu, J. Yang, Y. Zhang, C. Wang and D. Wang, *J. Appl. Electrochem.*, 2012, **42**, 989.

17　Y. B. He, B. Li, M. Liu, C. Zhang, W. Lv, C. Yang, J. Li, H. Du, B. Zhang, Q. H. Yang, J. K. Kim and F. Kang, *Sci. Rep.*, 2012, **2**, 913.

18　C.-W. Chen and M.-H. Lee, *Nanotechnology*, 2004, **15**, 480.

19　M.-F. Xu, Y.-J. Liao, F.-S. Zu, J. Liang, D.-X. Yuan, Z.-K. Wang and L.-S. Liao, *J.*

Mater. Chem. A, 2014, **2**, 9400.

20 Y. Gao, Z. Wang and L. Chen, *J. Power Sources*, 2014, **245**, 684.

21 P. Hohenberg and W. Kohn, *Phys. Rev.*, 1964, **136**, B864.

22 W. Kohn and L. J. Sham, *Phys. Rev.*, 1965, **140**, A1133.

23 G. Kresse and J. Furthmiiller, *Comp. Mater. Sci.*, 1996, **6**, 15.

24 P. E. Blöchl, *Phys. Rev. B*, 1994, **50**, 17953.

25 J. P. Perdew, K. Burke and M. Ernzerhof, *Phys. Rev. Lett.*, 1996, **77**, 3865.

26 L. Wang, T. Maxisch and G. Ceder, *Phys Rev B*, 2006, **73**, 195107.

27 S. Lutfalla, V. Shapovalov and A. T. Bell, *J. Chem. Theory Comput.*, 2011, **7**, 2218.

28 Z. Hu and H. Metiu, *J. Phys. Chem. C*, 2011, **115**, 5841.

29 S. L. Dudarev, G. A. Botton, S. Y. Savrasov, C. J. Humphreys and A. P. Sutton, *Phys. Rev. B*, 1998, **57**, 1505.

30 J. B. Goodenough and Y. Kim, *Chem. Mater.*, 2010, **22**, 587.

TOC Graphical Abstract for:

Workfunction, a new viewpoint to understand the electrolyte/electrode interface
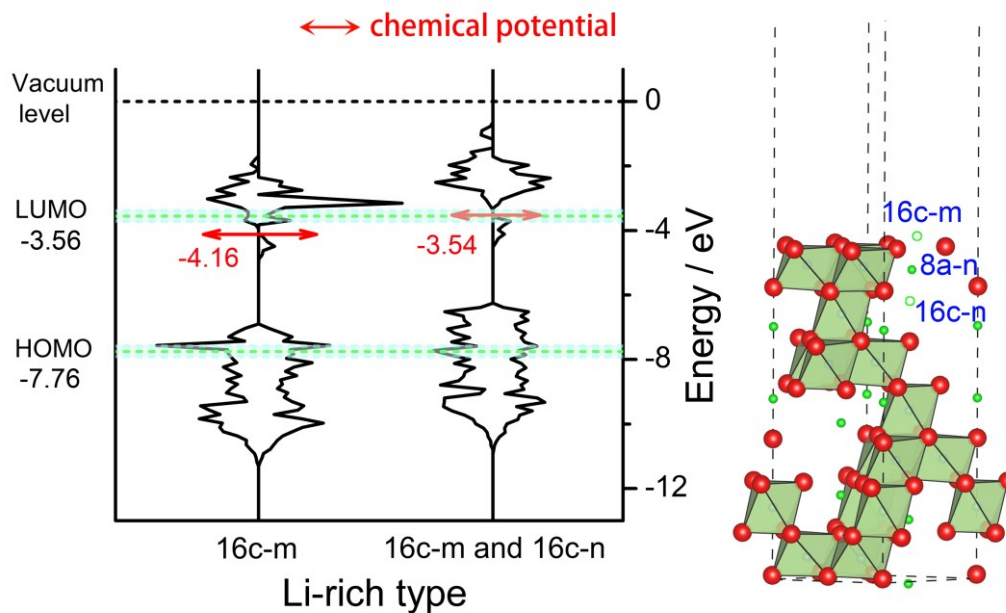
reaction

Li-rich surface of $Li_4Ti_5O_{12}$ triggers interface reaction transferring electrons from the Li-rich surface of $Li_4Ti_5O_{12}$ or $Li_7Ti_5O_{12}$ to the electrolyte.